Journal of Constructional Steel Research 206 (2023) 107937

Contents lists available at ScienceDirect

Journal of Constructional Steel Research

journal homepage: www.elsevier.com/locate/jcsr

Intensity and location of corrosion on the reliability of a steel bridge

Marco Simoncelli [a], Angelo Aloisio [b,*], Marco Zucca [c], Giorgia Venturi [a], Rocco Alaggio [b]

[a] Department of Architecture, Built Environment and Construction Engineering, Politecnico di Milano, Milan, Italy
[b] Department of Civil, Construction-Architecture and Environmental Engineering, University of L'Aquila, L'Aquila, Italy
[c] Department of Environmental Civil Engineering and Architecture, Università degli studi di Cagliari, Cagliari, Italy

A R T I C L E I N F O

Keywords:
Corrosion
Railway steel bridges
Reliability analysis

A B S T R A C T

Visual inspections generally represent the initial step of the safety assessment of bridges. In particular, steel railway bridges are particularly prone to corrosion phenomena. Therefore, visual inspections provide the geometric characterization of the conservation state of each structural member, in particular, the size reduction originating from the progress of corrosion. Nonetheless, the geometric definition of corrosion is not directly related to structural safety, depending on the damage location. The paper quantifies and discusses the uncertainties in the safety assessment of trussed bridges associated with the unknown effect of damage location on the stress distribution, given initial knowledge of the number and intensity of damaged members. Is it possible to preliminary assess the structural safety for typological structures without knowing the effect of damage location on the stress re-distribution? This paper discusses these aspects by randomly simulating damage scenarios in a finite element model of a historic steel bridge. The model, validated against the experimental modal parameters and measured deflection under train transit, is used for estimating bidimensional fragility curves as a function of the damage intensity and the number of damaged members. Finally, a safety domain can support the preliminary safety assessment of typological steel railway bridges.

1. Introduction

The safety of infrastructures such as bridges, viaducts, tunnels and dams must be an irrevocable requirement to preserve people's lives. Several structures have been in service for many years, and the maintenance state is often inadequate to guarantee a satisfying level of structural safety. Although periodic inspections of these structures must be continuously executed, they are often omitted due to economic and political issues. The lack of knowledge on the state of preservation is one of the major causes that leads to structural failure and global collapse. In the case of steel bridges, the principal source of material degradation is related to corrosion, which is an electrochemical reaction between the metal and the environment, that reduces the cross-section of the affected elements over time (Fig. 1), thus impairing their strength and ductility [1]. It is well-known that corrosion can affect the safety of concrete bridges by reducing the area of the steel rebars embedded into the concrete, as shown in [2–4] In steel bridges, deterioration due to corrosion can drastically reduce the bridge's life both limited to a local zone or along one or more elements [5–7] (Fig. 2).

Steel bridges were very popular in the past thanks to their relatively low cost and ease of fabrication. Therefore, an extensive heritage of ancient steel bridges is still in service. The deterioration of these strategic structures has hence become a great issue, independently of the construction material, especially in countries with a developed infrastructure network[8].

For the protection of steel bridges against corrosion, only coating was used in the past, but despite being easy to apply, it is obvious that the coating itself is subjected to deterioration and needs maintenance. Later, weathering steel was introduced into the market. Using corrosion-resistant alloys, such as stainless steel, is another approach to combat corrosion problems associated with classic carbon-steel bridges. However, due to the high cost compared with carbon steel, stainless steel has not yet gained a wide application in steel bridges. In recent years, a new type of corrosion-resistant steel, known as ASTM A709 Grade 50CR, has been proposed by ArcelorMittal. The advantages of this type of steel are discussed in Ref. [9]. Moreover, Soliman [10] presented an analytical investigation to quantify the life-cycle cost of a steel bridge constructed using conventional painted carbon steel and compared it with maintenance-free steel. Maintenance actions' indirect environmental, social, and economic impacts are computed to quantify the sustainability metrics associated with steel bridges during their life cycle. The proposed results are applied to a bridge located in the USA. It has been shown that although corrosion-resistant steel has a higher initial cost, its life-cycle cost is less than that of the conventional steel.

* Corresponding author.
E-mail address: angelo.aloisio1@univaq.it (A. Aloisio).

https://doi.org/10.1016/j.jcsr.2023.107937
Received 28 January 2023; Received in revised form 27 March 2023; Accepted 28 March 2023
Available online 3 April 2023

Fig. 1. Local corrosion of steel elements (original figures not related to the case study).

Fig. 2. Corrosion through a whole steel element (original figures not related to the case study).

Many authors proposed different numerical and experimental strategies to carry out an overall estimation of the bridge life. Gardoni et al. [11] proposed a Bayesian methodology to develop seismic fragility curves of bridge components in case of corrosion. The method was applied to two concrete bridges. The proposed models can be used to existing and new concrete columns to study the sensitivity of such elements to corrosion. In [12,13], an efficient procedure for the collapse mechanism evaluation of existing RC bridges under horizontal loads is presented by considering different scenarios of corrosion. The bridges were investigated using a multi-modal pushover method of analyses considering brittle and ductile failure mechanisms. It has been shown that low corrosion levels lead to negligible reductions in the steel rebar area and do not influence the values of the risk indices. On the contrary, high corrosion levels significantly influence the values of the risk indices, leading to the activation of brittle collapse mechanisms for peak ground accelerations much lower than those prescribed by the Italian Code for the sites where the bridges are located. Similar studies were conducted on steel bridges [14] by estimating the fatigue life of corroded bridges based on finite element predictions. Corrosion was modelled by considering a uniform corrosion distribution along the cross-section. Different methods for predicting the bridge's remaining life were then shown.

The combination of the three sources, visual inspections, continuous monitoring and the finite element (FE) model represents the key to successfully evaluating the structural condition of a bridge [15–17]. Visual inspections are the most widespread and default method for assessing the safety of a structure. However, if predictions do not support it, it is challenging to formulate a reliable and objective judgement of the structural state [18]. As highlighted by a Federal Highway Administration (FHWA) report [19], the main drawbacks of visual inspection affect the timing (limited agility of the response in maintenance and rehabilitation decisions), interpretability (subjective assessment), and accessibility (possible lack of a clear line of sight for condition assessment). Regrettably, no universally accepted nondestructive testing methods or equipment complement visual inspection in situations where visibility is an issue. Thus, accessibility is a significant consideration in assessing the effectiveness of visual inspection in general. Continuous monitoring is widespread. There are countless Structural Health Monitoring (SHM) sensing technologies, both emerging and established that may be considered for bridge monitoring [20–22]. The typical instrumentation is strain gauges and accelerometers, widely used for decades to measure structural responses [23]. More recently, optical-fibre sensors have been applied for strain, temperature, and vibration measurement [24]. Fibre-optic sensors are less susceptible to electrical noise and can provide distributed measurements along the structure, in contrast to the discrete nature of strain gauges and accelerometers [25,26]. Researchers have also proposed using applied coatings to indicate structural changes. These coats may provide visual cues resulting from property changes in response to structural changes [27,28]. Measuring bridge deflections can be problematic because a fixed reference point is needed. Nonetheless, the damage sensitivity features extracted from the accelerometers are less sensitive to damage than bridge deflections [29]. Therefore, alternative approaches have been developed to measure deflection using GPS [30] directly, radar-based systems [31], video [32], laser-based systems [33] or unmanned aerial vehicle [34,35]. However, despite spreading the monitoring systems, there are several unclear aspects in the structural health monitoring paradigm. The most critical element is bridging the gap between anomaly detection and the remaining life of a structure [36]. Secondarily, there is no unique recipe for extracting the damage-sensitive features, which vary from case to case, depending on the structural system and the chosen monitoring approach. Additionally, A FE model is necessary to predict damage scenarios that represent the object of the activity despite being unlike to occur. The complexity of the problem demands multi-criteria and multidisciplinary approaches. The issues related to the service life prediction of steel bridges are complex. Nonetheless, detailed analyses of case studies help understand the best and most informative methods for assessing the structural state, trying to combine traditional methods based on visual inspections and instrumental ones based on continuous monitoring. The objectives of this study are twofold; see Fig. 3:

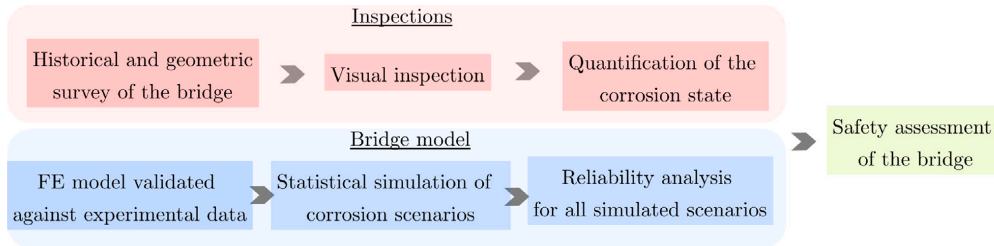

Fig. 3. Workflow of the safety evaluation approach.

Fig. 4. Views of the steel truss bridge without ballasted track.

- proposal of a preliminary safety-assessment approach based on visual inspections and statistical indicators obtained from random simulations of damage scenarios;
- sensitivity of a set of damage-sensitive features to the intensity and location of corrosion. This step highlights the most informative measurements to be retrieved from this structure.

The paper presents a novel strategy to correlate visual inspection directly to structural safety. The case study is a steel railway bridge built in Italy in the 50 s. A structural model has been created and then validated by comparing the results obtained from the model with the experimental ones (Section 3). Subsequently, different models have developed: a bridge in the ideal situation, i.e. no corrosion, and a bridge with varying scenarios of corrosion. For all the considered scenarios, static, buckling and modal analyses have been executed, performing the safety checks required by the Italian code [37] regarding maximum deflection and capacity factor. Fragility curves were developed by relating structural safety with the number of corroded elements and corrosion penetration. Finally, a practical chart, derived from the fragility curves, is proposed and discussed, which can be used for preliminary consideration of the bridge's safety.

2. Case study

The case study is a three-span bridge along an Italian railway line. This paper does not provide an exact safety assessment of the bridge in its actual state, which is not the object of this research. The authors only use this case study to demonstrate a possible approach for preliminary safety assessment based on the outcomes of visual inspections. The discussed results should always be considered in comparative terms.

2.1. Bridge description

The central and side spans are steel trusses equal to 52 m and 24 m, respectively (Fig. 4). The authors focused on the response of the side spans since the central span crosses the river and is not accessible for direct displacement measurement. The bridge has no ballast and has the direct laying of wooden sleepers. The masonry substructures support the steel beams laid directly on a pulvinus of large squared stone blocks.

The side spans of the bridge have an open-deck structure with the following composition (Fig. 5):

- The lower and upper chords have a mutual extrados distance equal to 3.00 m. They consist of a double T profile with a nailed section and a 400 mm high core. The profiles have a variable section, with overlapping plates constituting the flanges approaching the centre line (Fig. 5a).
- The vertical members have a double L profile. They are fastened with rivets to the plates supporting the diagonal members (Fig. 5b).
- The X-shaped diagonal members are composite elements made of four conventional UPN profiles with variable height coupled by steel plates. Two UPN profiles have flanges arranged inwards to obtain the connection of the diagonals by the intersection, while the other two have flanges oriented outwards. The profiles vary in size, ranging from 180 mm to 220 mm in height by the supports (Fig. 5c).
- There are nine stringers, two by the span edges, consisting of a double T nailed profile with an 800 mm height, with a 3.00 m mutual distance (Fig. 5d).
- The spars have a double T nailed profile with a 500 mm height (Fig. 5e), with mutual distance, almost coinciding with the track gauge (1520 mm);
- The lower horizontal bracing consists of angular profiles connected at the cross knot — longitudinal beam just above the wing of the lower bridle. The two profiles are connected at the intersection with a single nail;
- There are no bracings of the spars, but simple crosspieces placed a half of the span in correspondence of each section identified by two consecutive stringers.

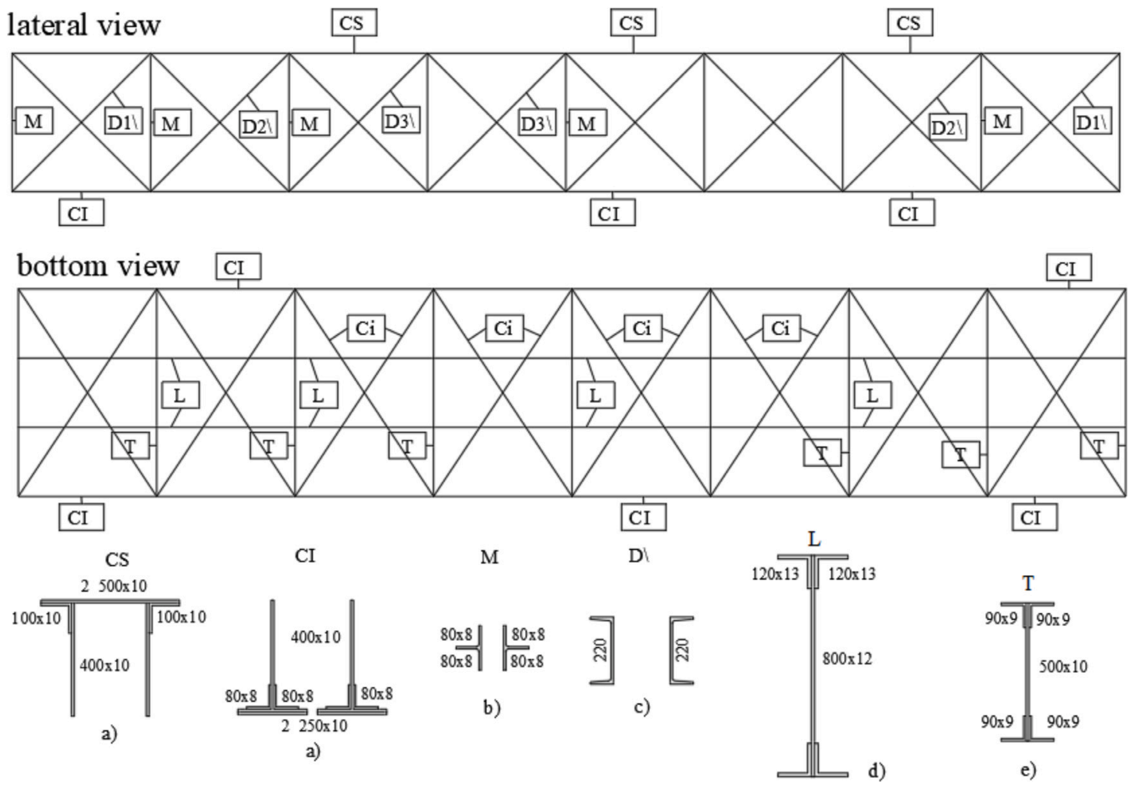

Fig. 5. Cross-sections of the lateral span of the considered bridge.

3. Dynamic identification and model validation

The numerical model has been validated by using two different experimental techniques: dynamic identification and quasi-static tests. Therefore, two sets of experimental data were used (experimental modal shapes and frequencies and the mid-span deflection under a trainload) to double-validate the model's accuracy under the excitation of both ambient and trainload.

3.1. Experimental modal analysis

The experimental layout consists of two rows of seven equally-spaced Force Balance Accelerometers (FBA) [38,39]. The digital array accelerometric measurement chain comprises SL06 converters and FB SA10 accelerometers produced by Sara Electronic Instruments (Italy). The accelerometer has a dynamic range higher than 165 dB from 0.1 Hz to 20 Hz with 1 g full scale. On the other hand, the dynamic range of the digital converter is 144 dB, such that the sensitivity is limited by the converter, not by the noise of the accelerometer, which is lower. Accordingly, the sensitivity of the sensor is 0.119 μg/count. The accelerometers were arranged into two measurement chains, each driven by a master recording unit connected to a Wi-Fi access point and synchronized by GPS receivers, see Fig. 6.

The dynamic tests were carried out under ambient excitation. The time series is about 20 min long. The modal parameters are estimated using the covariance-driven Stochastic Subspace Identification (SSI) method [40,41]. The data were sampled at a rate of 200 Hz. The preprocessed data were used for SSI and subsequent modal analysis, resulting in eigenfrequencies, damping ratios, mode shapes and covariances of these modal parameters for each setup. The time shift and maximum model order are equal to 6, and 150 [42]. The data were decimated with a decimation factor equal to 4.

Table 1 lists the stable modes obtained from the dynamic identification; see the stabilization diagram in Fig. 6(c). Fig. 7 displays the tridimensional plots of the experimental modes.

Table 1
List of the experimental (f) and numerical natural (f_{num}) frequencies, damping ratio (ξ) and MAC of the identified six stable modes. The MAC is estimated between the experimental and numerical mode shapes.

No	f [Hz]	ξ [%]	f_{num} [Hz]	MAC
1	5.59	0.33	6.14	0.92
2	10.04	1.1	10.67	0.88
3	11.27	0.79	11.81	0.93
4	12.34	0.67	14.35	0.98
5	15.04	0.14	–	–
6	16.99	0.33	16.81	0.97

The first mode at 5.589 Hz is bending-torsional, with dominant components along the y and z directions. The vertical displacement at the support is almost null, resembling a pinned-pinned connection. The second mode at 10.04 Hz is the first vertical bending mode with negligible components in the x–y plane. The mode is highly symmetric, also proving structural symmetry. The third mode at 11.27 Hz is an almost pure torsional, with negligible components along the y and x axes. The fourth mode at 12.34 is very similar to the first mode. It has prevalent displacement in the z-axis, looking like a first torsional mode. However, as highlighted in Fig. 8, the main difference between the first and the fourth modes stands in the in-plane deck deformation. The first mode has no in-plane components, with prevalent mode deformation in the z-direction. Conversely, the fourth is a bending-torsional model, exhibiting a significant bending deformation in the deck plane.

The stabilization diagram shows two close alignments at 15.04 and 15.33, respectively. The mode shape associated with 15.04 Hz is challenging to interpret, and possibly, it is a non-physical mode due to the higher complexity. Conversely, the mode at 15.33 Hz resembles another manifest torsional mode with prevalent deformation in the z-direction. Compared to the first and the fourth, as highlighted in Fig. 8, the main difference stands in the in-plane deformation, exhibiting a second-order in-plane bending.

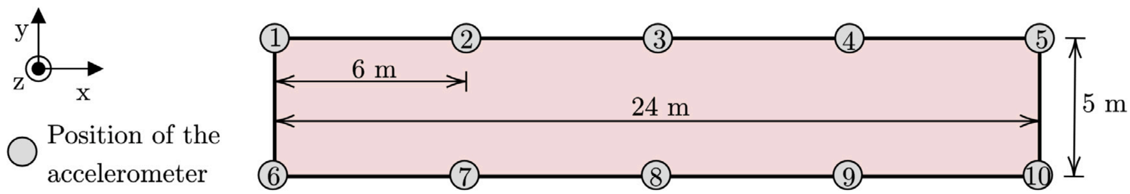

(a)

(b)

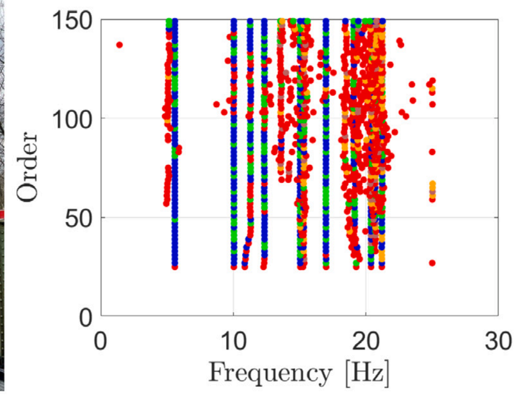

(c)

Fig. 6. (a) Layout of the accelerometers; (b) Experimental setup; (c) Stabilization diagram. The colour legend for the stabilization diagram is the following. Red-unstable; orange-stable in frequency; brown-stable in frequency and damping; blue-stable in frequency and shape; green-stable in frequency damping and mode shape. Regarding the stabilization criteria, the thresholds corresponding to the relative variation of the MAC, frequency and damping were set equal to 0.02, 0.01 and 0.01, respectively.

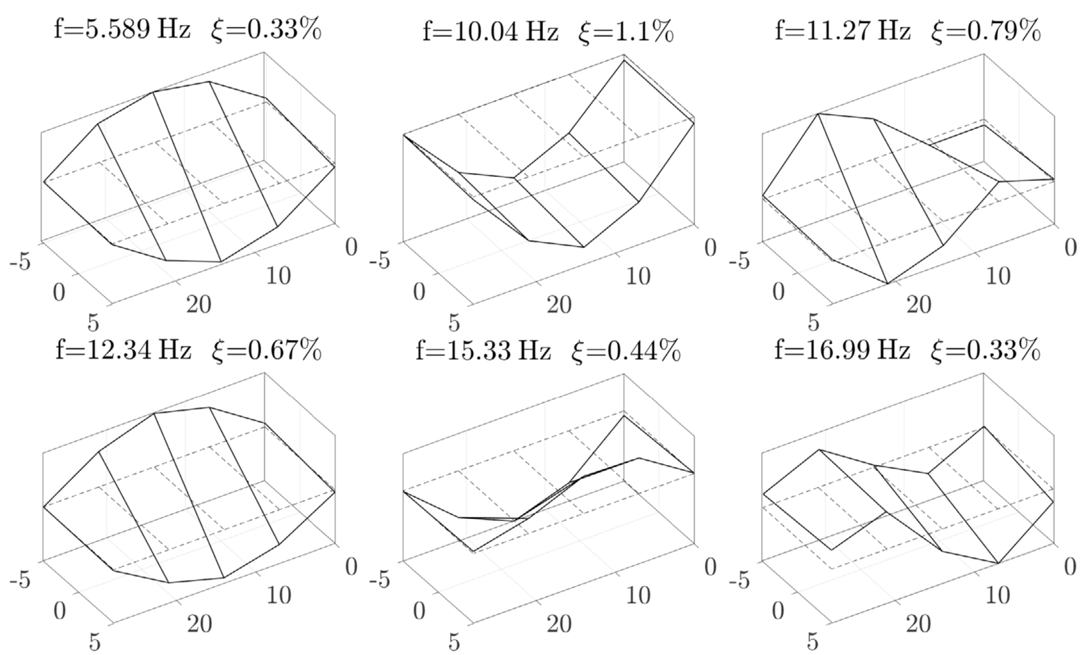

Fig. 7. 3D plot of the experimental modes.

The sixth mode at 16.99 Hz is a second vertical bending mode, with prevalent displacement in the z direction. Moreover, the numerical modal results are also depicted in the same Table 1. In particular, the numerical frequencies (f_{num}) are reported together with the Modal Assurance Criterion (MAC) coefficient. The MAC(i,j) has the form of a coherency coefficient between the numerical mode i and the experimental j one, and it ranges from 0 (no correlation) to 1 (numerical data fits perfectly with the experimental ones). A MAC value greater than 0.80 is generally considered a good match, while a MAC value less than 0.40 is considered a poor match. It should be noted that the numerical model can predict the bridge's modal response, giving a MAC index always higher than 0.88 with the difference between the frequency consistently lower than 10%. The fifth experimental mode is not present in the numerical ones. All the numerical modes are depicted in Fig. 9, showing that the numerical shapes agree with the related experimental ones.

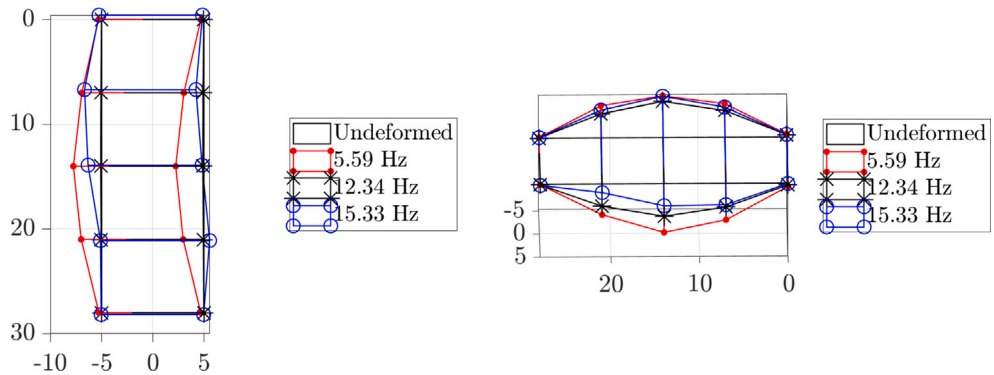

Fig. 8. Comparison between the first, fourth and fifth modes. (a) Top and (b) lateral views of the mode shapes.

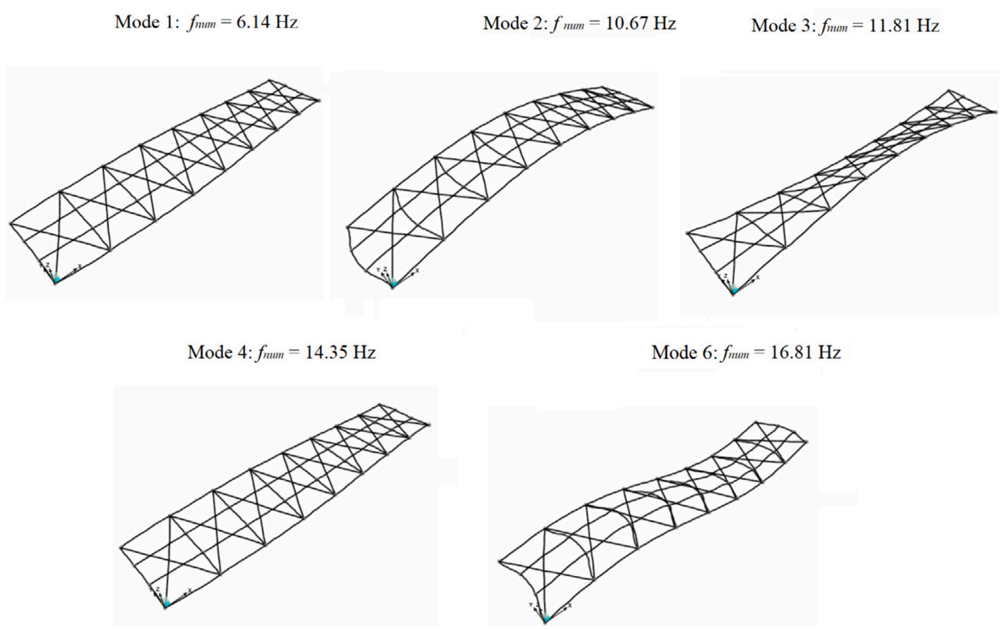

Fig. 9. 3D plot of the numerical modes.

3.2. Experimental displacement response

The experimental equipment consisted of two easels supporting a laser sensor. The laser sensors are Micro-epsilon optoNCDT 1420 [29]. The sampling rate is 1000 Hz. The C-Box/2 A controller (Micro-epsilon) synchronizes and digitizes the two signals acquired by a personal computer from an Ethernet cable. A lead–acid battery provides power to the laser sensors, the controller and the personal computer. The two lasers measured the displacement response at the edges of the mid-span cross-section. Fig. 10 shows the experimental setup for the considered bridge.

Fig. 12 shows the experimental displacement response of the bridge under two identical trains moving at a quite low velocity:30 km/h. The train consists of a locomotive and a single car. The maximum load is obtained when both the car and the locomotive are on the bridge, as shown in Fig. 11. It must be remarked that the length of the car and the locomotive is larger than the bridge span. The displacement response has three local maxima. The first maximum corresponds to the presence of the first axis of the first car; the maximum peak corresponds to two axes crossing the bridge, while the third is associated with the third axis leaving the bridge. The maximum deflection in both cases is, on average −3.28 mm (Fig. 12(a)) and −3.37 mm (Fig. 12(b)). Despite, theoretical and experimental evidence proved that free oscillations could occur after the train passage [43], in this case, there are no free oscillations as the train leaves the bridge. This depends on the relatively low speed of the train. The train load is centred on the bridge's longitudinal axis. This fact is confirmed by the absence of notable differences among the displacement responses measured at the two edges of the mid-span cross-section. Considering the low velocity of the train and the absence of free oscillation after the test, the experiment can be classified as quasi-static. For this reason, a static load has been applied in the numerical model. The static load has been applied as a single concentrated load by the midspan, corresponding to the case in Fig. 11. This condition maximizes the bridge deflection in this loading scenario. The load is obtained by summing the nominal values for the weight of the locomotive and the car, equal to 850kN. In Fig. 12, the numerical result is reported with a continuous horizontal line: the maximum numerical displacement is almost 14% greater than the numerical one, confirming the relatively good agreement between numerical and experimental also in quasi-static (static) load conditions.

4. Parametric analysis

A parametric analysis was executed to determine the corrosion effect on the bridge response. Different corrosion scenarios were applied to start from the previously validated FE model. The effect of

Fig. 10. Experimental setup; (b) View of the bridge under a two-cars train transit moving at 30 km/h.

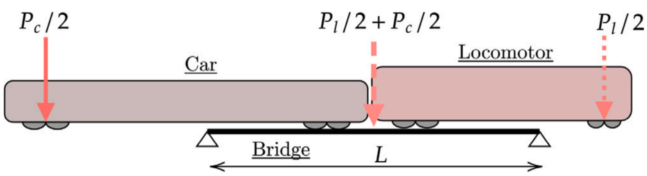

Fig. 11. Representation of the applied loads in the FE model, where $P_l = 1200$ kN is the weight of the locomotive, and $P_c = 500$ kN is the car's weight.

corrosion spreading along a single element and on different elements simultaneously (two to four members) was simulated. All 42 beams on each side were considered by varying the corrosion position. According to the literature studies [14], the corrosion was considered uniformly distributed along the cross-section under investigation. The corrosion effect was assumed to be a reduction of the cross-sectional area. Seven different percentages of the loss Area were considered, ranging from 10% to 70%. The not-corroded case (0% loss area) was always considered a comparative term. It is worth underlining that when an element is corroded, all its length is considered corroded, and no local effects were implemented. By combining all the scenarios, more than 1000 different models were created. Fig. 13 presents the synopsis of the considered models.

It should be remarked that for all the models, static and modal analyses were performed monitoring the natural frequency of vibrations (f_i), the maximum vertical displacement (d_s) at the elastic limit state (SLS) and the Safety Index (SI), of all the elements, at the ultimate limit state (ULS). Local effects of the corrosion were not investigated in the paper and consequently the corrosion was assumed uniform on the element without modifying the element buckling length. This aspect would be further investigated in future works.. The load history was assumed according to the Italian national code for railway bridges, consisting of a moving load composed of mixed distributed and concentrated forces (resulting in higher values than the one used for the model validation) [37]. Regarding evaluating the SI, EUROCODE-3 [44] was considered. As discussed in Section 2, the bridge elements were characterized by different cross-sections: some can be classified as bi-symmetric cross-section members, and others must be considered mono-symmetric cross-sections (with all the associated problems related to the torsional behaviour). The SI is defined as:

$$SI_1 = \frac{N_{Ed}}{\chi_y N_{Rd}} + k_{yy}\frac{M_{y,Ed}}{\chi_{LT} M_{y,Rd}} + k_{yz}\frac{M_{z,Ed}}{M_{z,Rd}} \tag{1}$$

$$SI_2 = \frac{N_{Ed}}{\chi_z N_{Rd}} + k_{zy}\frac{M_{y,Ed}}{\chi_{LT} M_{y,Rd}} + k_{zz}\frac{M_{z,Ed}}{M_{z,Rd}} \tag{2}$$

where N_{Ed}, $M_{y,Ed}$, $M_{z,Ed}$ and N_{Rd}, $M_{y,Rd}$, $M_{z,Rd}$ are the design and the resistance values of the compression and the bending moments about the principal axes, respectively; χ_y and χ_z are the reduction factors due to the global flexural buckling. In the case of open mono-symmetric members, flexural–torsional buckling can occur, and the associated reduction factor χ_{FT} must be accounted for; χ_{LT} is the reduction factor associated with the lateral torsional buckling. Finally, k_{yy}, k_{yz}, k_{zy} and k_{zz} are the interaction factors defined in accordance with [44].

The safety of a member is guaranteed if the following relationships are satisfied:

$$SI = max(SI_1; SI_2) \leq 1 \tag{3}$$

In addition, also the buckling elastic multiplier at the ultimate limit state has been evaluated for all the models (α_{cr}). The buckling multiplier has been assumed as the minimum positive global buckling value among the ones obtained from the buckling analysis of the models obtained from the solution of the eigenvalue problem:

$$det([K_E] - \lambda[K_G])\Phi = 0 \tag{4}$$

$$\alpha_{cr} = min(\lambda(i)) = 0 \tag{5}$$

where K_E is the global elastic stiffness matrix, K_G is the global geometric stiffness matrix, λ is the vector which contains all the buckling multipliers, and Φ is the matrix which contains the eigenmodes associated with each buckling multiplier.

Finally, an automatic procedure to estimate the modal accuracy has been developed. The modal accuracy has been estimated by weighing the MAC coefficient, evaluated between each numerical mode of each model and the experimental values, with the corresponding difference in frequencies. An accuracy matrix, ACC (i,j), was hence defined [45]:

$$ACC(i,j) = \frac{min(f_{num}(i), f(j))}{max\,f_{num}(i), f(j)} \cdot \frac{mass(i)}{mass_{tot}} \cdot MAC(i,j) \tag{6}$$

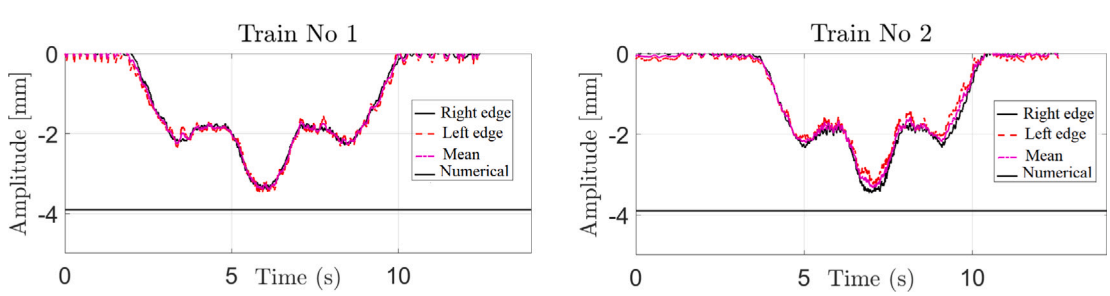

Fig. 12. Mid-span deflection under two train transit. The two trains are nominally identical with a 30 km/h speed.

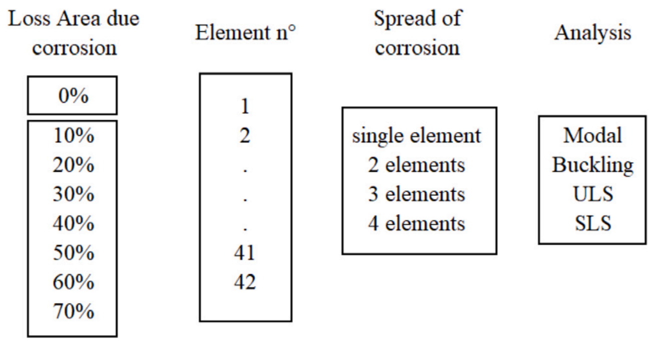

Fig. 13. Layout of the considered models.

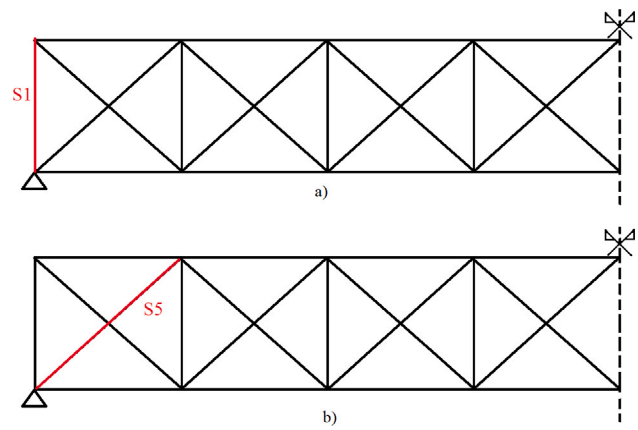

Fig. 14. Scenario 1 (a) and scenario 5 (b) for the case of 1 element corroded. With the red colour, the corroded element is indicated.

where *mass(i)* is the participating mass related to the specific modal shape. The final accuracy value is obtained from the selection of all the maximum factors belonging to the ACC(i,j) matrix:

$$ACC_{max}(i) = maxACC(i,j)withj \in 1,2,\dots.M \tag{7}$$

$$ACC = \sum_{1}^{N} ACC_{max}(i) \tag{8}$$

The model can be considered accurate when the ACC is 0.8–1.0 [45].

4.1. 1 Element corroded

A single element has been corroded, and its position was changed along the bridge, generating 42 scenarios. As discussed, seven different percentages of loss area were considered for each scenario. To clarify the procedure, 2 of 42 scenarios are depicted in Fig. 14.

The results associated with the 1-element scenarios are presented in Fig. 15. The figure is divided into four subplots representing: the maximum SI, the maximum displacement over the displacement limit of NTC18 for such bridges, the buckling multiplier and the modal accuracy. Blue points are related to each scenario, while the red line represents the mean values between the 42 scenarios connecting the different percentages of loss area. Finally, with the horizontal black straight line, the acceptability limit of the single parameter is reported (e.g. for the SI, the value that should not be exceeded is set to 1). For the Modal accuracy, the two black straight lines highlight the range 0.8–1.0.

As shown in Fig. 15 the influence of a single corroded element on the global response of the bridge is quite limited. In fact, by observing the results in terms of Modal accuracy and elastic buckling multiplier, it can be noted that there is no sensible variation of the values, independently of the position of the corroded element. Also, by looking at the mean values associated with the displacement ratio and with the SI distribution, it can be stated that no significant variation in the results was observed. More in detail, the increasing of the % of corrosion on the elements brings to more scattered values, especially in the SI graph. It should be remarked that, with a high level of corrosion, some scenarios bring to an SI >1, i.e. for the specific scenario, the safety check of the bridge at ULS is not satisfied. This means that if after a visual inspection, at least one element can be found with a high level of corrosion (loss area >60%), an accurate FE analysis is necessary to establish the safety of the infrastructure.

Table 2
Median values of the results with multi-element corroded (2,3 and 4 elements corroded simultaneously).

Safety parameter	Loss Area						
mean value	10%	20%	30%	40%	50%	60%	70%
SI	0.91	0.91	0.91	0.91	0.92	0.92	0.92
d_s/d_{NTC}	0.65	0.66	0.66	0.67	0.68	0.69	0.71
α_{cr}	52.9	52.7	52.5	52.1	51.5	50.2	46.6
ACC	0.89	0.89	0.89	0.89	0.90	0.98	1.00
SI	0.91	0.91	0.91	0.91	0.92	0.92	0.92
d_s/d_{NTC}	0.66	0.66	0.67	0.67	0.68	0.71	0.74
α_{cr}	52.9	52.6	52.1	51.5	50.4	47.3	42.6
ACC	0.89	0.89	0.89	0.89	0.90	1.00	1.00
SI	0.91	0.91	0.91	0.91	0.92	0.92	0.92
d_s/d_{NTC}	0.66	0.66	0.67	0.68	0.70	0.72	0.76
α_{cr}	52.9	52.4	51.8	51.1	49.5	46.2	40.6
ACC	0.89	0.89	0.89	0.93	1.00	1.00	1.00

Table 3
Standard deviation of the results with multi-element corroded (2,3 and 4 elements corroded simultaneously).

Safety parameter	Loss Area						
st.dev	10%	20%	30%	40%	50%	60%	70%
SI	0.0060	0.0115	0.0127	0.0149	0.0186	0.0250	0.0387
d_s/d_{NTC}	0.0012	0.0026	0.0046	0.0071	0.0107	0.0161	0.0248
α_{cr}	0.2865	0.6387	1.0799	1.6471	2.4037	3.6034	5.6527
ACC	0.0007	0.0016	0.0026	.0040	0.0645	0.0915	0.0832
SI	0.0066	0.0128	0.0145	0.0159	0.0180	0.0215	0.0282
d_s/d_{NTC}	0.0012	0.0028	0.0048	0.0076	0.0107	0.0161	0.0246
α_{cr}	0.2565	0.5693	0.9844	1.6471	2.359	4.1874	6.6627
ACC	0.0007	0.0014	0.0022	.0404	0.0905	0.0915	0.0742
SI	0.0071	0.0138	0.0159	0.0166	0.0180	0.02110	0.0268
d_s/d_{NTC}	0.0015	0.0034	0.0059	0.0092	0.0139	0.0209	0.0324
α_{cr}	0.2896	0.6387	1.0639	1.5881	2.2393	4.5034	7.0002
ACC	0.0008	0.0017	0.0027	0.0740	0.0855	0.0815	0.0642

4.2. Multi-elements corroded

The same procedure showed for one by one corroded element was replied by considering the simultaneous corrosion of 2,3 or 4 elements. An example of two scenarios with 4 corroded elements is reported in Fig. 16, in which the corroded elements are reported with the red colour.

Also, for these cases, all the checks have been performed. For the sake of brevity, in Fig. 17, only the results associated with 4 elements corroded simultaneously are depicted. Moreover, the complete summary of all the scenarios is reported in Tables 2 and 3 depicting the mean values and the standard deviation, respectively.

Independently of the number of corroded elements when the loss area is lower than 20% the influence on the global response is quite limited in terms of both mean values and standard deviation of each parameter. With 3 and 4 corroded elements, increasing the percentage

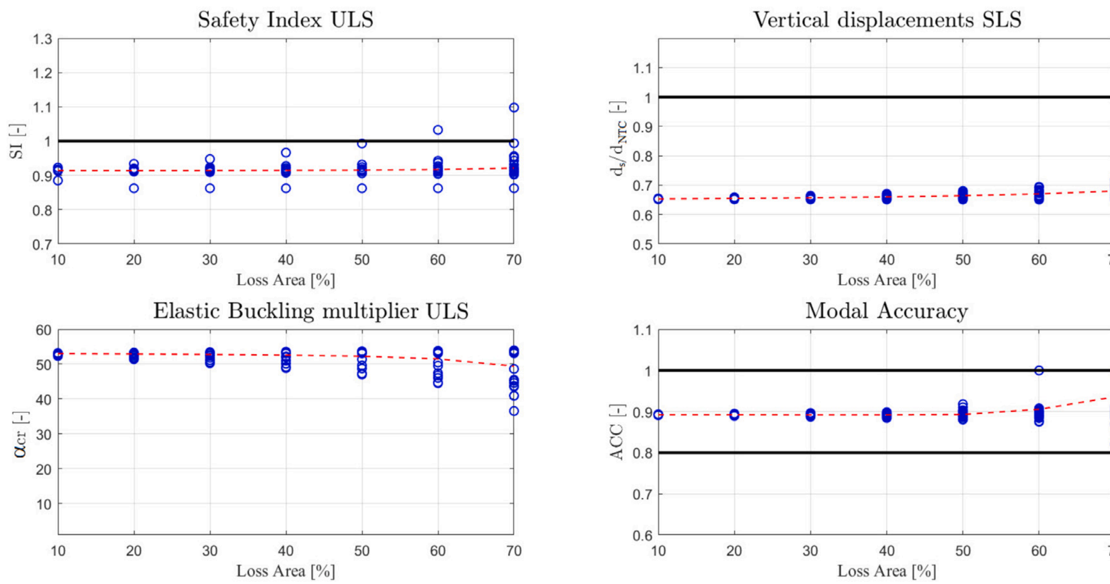

Fig. 15. Results with one element corroded. The blue dots represent the results associated with each considered scenario. The red dashed line is the mean value among the considered scenario, while the continuous black lines highlight the safety or acceptability limit of the specific parameter.

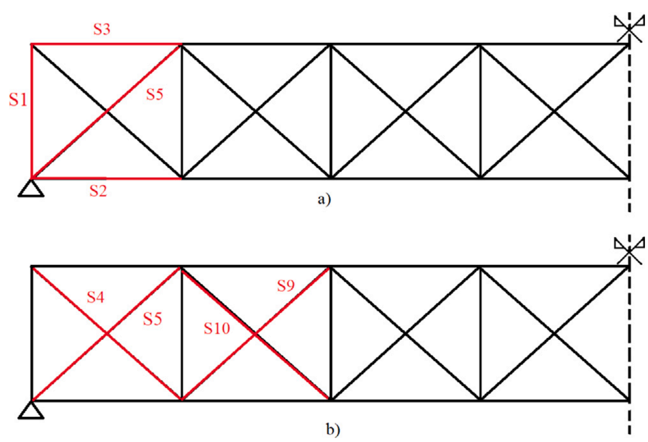

Fig. 16. Two scenarios with 4 elements corroded. Red lines represent the corroded elements.

of corrosion up to 50%, the value of the standard deviation (i.e. the dispersion of the results from the mean) dramatically increases, revealing that some scenarios become less safe than others, bringing to an early global collapse of the bridge. This significant result can reveal that such a statistical approach maintain its validity only when the number of simultaneously corroded element is limited, and the level of corrosion is low. The observation of the SI reveals that when the corrosion percentage increases, more elements along the bridge overpass the safety limit of 1. Finally, an important conclusion that can be assessed from the proposed scenarios is that with a high level of corrosion and four corroded elements, the evaluation of the modal parameters cannot give a precise prediction of the state of damage of the bridge. On the contrary, the assessment in terms of global displacements can give an accurate indication for the safety evaluation of the bridge.

5. Fragility estimate

The limit state function of the bridge can be formulated as

$$g(\mathbf{x}, \mathbf{p}, \boldsymbol{\Theta}) = C(\mathbf{x}, \mathbf{p}, \boldsymbol{\Theta}) - D(\mathbf{x}, \mathbf{p}, \boldsymbol{\Theta}) \tag{9}$$

where $C(\mathbf{x}, \boldsymbol{\Theta})$ is the capacity, $D(\mathbf{x}, \boldsymbol{\Theta})$ is the demand obtained from the given traffic scenario, $\mathbf{p}$ collects the known parameters of the structural model, $\mathbf{x} = \{n_d, s_d\}$ collects the damage parameters in terms of number (n_d) and size reduction (s_d) of the damaged members, and $\boldsymbol{\Theta} = \{\theta, \sigma\}$ are unknown model parameters. The limit state function can be used to compute the fragility of a given structure. Fragility functions define the conditional probability of meeting or exceeding a prescribed limit state for a given value of the demand measure. The number of damaged members and the entity of damage ($\mathbf{x}$) can be considered suitable intensity measures for fragility estimation. The intensity measure used for the fragility estimation is the load multiplier γ. The events associated with a limit state function less or equal to zero define the failure related to the considered phenomenon. Rigorously, following Eq. (9) the fragility of a given structure can be written as

$$F(\mathbf{x}, \mathbf{p}, \boldsymbol{\Theta}) = P\left[\{g(\mathbf{p}, \boldsymbol{\Theta}) \leq 0\} \,|\mathbf{x}\right] \tag{10}$$

Empirical fragilities are estimated using direct Monte Carlo simulations. The failure probability is obtained by dividing the number of simulations associated with exceeding the number of cycles to failure and the total number of simulations.

Uncertainty affecting the vulnerability of a structure can be categorized as epistemic or aleatory. The latter represents the intrinsic causality associated with natural phenomena and cannot be easily governed. On the contrary, the epistemic uncertainty is related to the lack of knowledge and hence can be investigated by changing selected parameters in the numerical model. The paper focuses on epistemic uncertainty in the parameters related to bridge material information, an uncertainty that has, of course, an influence on the resulting fragility curves. As discussed in the first section, since these kinds of bridges are generally old structures, it is not easy to have information on the actual properties of the material used for the construction. For this reason, to estimate worthy fragility curves, together with the variation of the damage and its position, the material was changed, considering a variation on the Young modulus (E) and on the yielding stress (f_y). The parameter variation for the statistical simulation is reported in Table 4.

For each numerical model, starting from the NTC configuration, the concentrated and distributed applied load have been increased by varying a multiplier γ coefficient (vertical load multiplier) from 0.8 to 2.0. Two different limit states have been considered: SLS, the limit is reached when the maximum displacement is greater than the one admitted by NTC18, i.e. when $d_s/d_{NTC} > 1$; ULS, the limit is reached

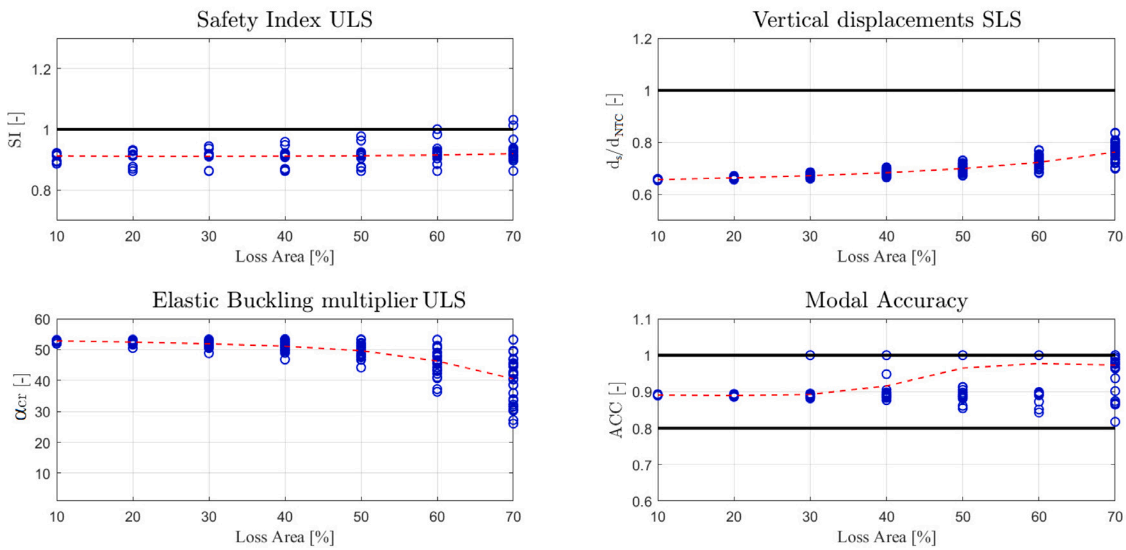

Fig. 17. Results with 4 elements corroded. The blue dots represent the results associated with each considered scenario. The red dashed line is the mean value among the considered scenario, while the continuous black lines highlight the safety or acceptability limit of the specific parameter.

Table 4
Input parameters for the Monte-Carlo simulation, where CoV is the Coefficient of Variation.

Variable	Distribution	Parameters	
Simultaneously corroded	Uniform	Lower Bound: 1	Upper Bound: 4
Loss area [%]	Uniform	Lower Bound: 10	Upper Bound: 70
E [GPa]	Normal	Mean: 210	CoV: 0.05
f_y [MPa]	Normal	Mean: 275	CoV: 0.05

when one element overpass the stability limit, i.e. SI > 1. It can be noted that, at the ULS, the capability of the bridge to redistribute internal forces, when a specific element collapses, is not accounted for. This assumption is in accordance with the safety rules imposed by the [37,44]. However, this conjecture makes it impossible to follow the phases that characterize the bridge's progressive collapse. In Fig. 18 the mean fragility curves which relate the probability of the bridge collapse, P(x), and the vertical load multiplier, γ, are depicted divided by the number of simultaneously corroded elements: Fig. 18a); only one corroded element; Fig. 18b) two elements corroded; Fig. 18c) three elements corroded and Fig. 18d) four elements corroded. For the sake of clarity, the boundary of the analyses associated with the uncertainty of the material properties is not shown in the figure. As expected, all the fragility curves assume a quite straight vertical shape, which denotes a sudden collapse once the maximum load is reached. The fragility curves become smoother with the increase of corrosion.

By looking at a 50% probability of collapse, it can be noted that for the case of 1 element corroded independently on the percentage of the loss area, the bridge load multiplier is quite higher than the one, ranging from 1.46 to 1.53. On the contrary, by observing the case with 4 elements corroded simultaneously, the loss area greatly influences the results since the load multiplier ranges from 1.3 to 1.53.

Finally, for the ULS limit state Fig. 19 can be considered. It can be noted that also, in this case, all the curves are quite vertical, independently of the percentage of corroded area. All the curves are overlapped and around the load multiplier of 1. It should be noted that such an approach can give an initial estimation of the state of the safety of the bridge by combining statistical predictions with visual inspections. In reality, when multi-corroded elements are detected, the state of damage of each element can be different. To consider this situation, a 3D fragility representation is necessary, which combines the safety level at the same time with the number of corroded elements and the percentage of the loss area. In this view, Fig. 20 represents a possible practical tool for directly assessing the safety reduction due to the level of corrosion and the number of corroded elements. The contour plot shows the load multipliers corresponding to a given reliability value, 3.8 in (a) and 4.2 in (b). Therefore, the above representations represent a decision-making tool. Given the observations regarding the number of corroded elements and the percentage of corrosion, the reduction of the permissible load on the bridge can be estimated. Accordingly, estimating the admissible load for a given reliability index can limit train traffic in terms of velocity and weight so that the reduced allowable loads are not exceeded.

6. Conclusions

Due to their past popularity, there is a large heritage of ancient steel bridges, still in-service, which need maintenance. A large number of these bridges are used as railway bridges and, in many cases, their level of safety has not been always deeply investigated. Indeed it is well-known that one of the main problems which greatly affects the stability of such steel structures is the corrosion of the members and for this reason, many researchers are trying to develop a reliable method to predict the residual life of corroded steel bridges. The first tool which can give information to the designers on the state of conservation of these infrastructures is the visual inspection. The survey must be always followed by a safety evaluation of the bridge in the corroded configuration, via numerical or theoretical analyses. However, this step can be a big issue because of the lack of information and uncertainties associated with old structures.

In the paper, a practical chart is proposed to directly connect visual inspection and safety checks based on statistical fragility estimation of the bridges. In particular, the proposed methodology has been applied to a railway-trussed steel bridge, located in Italy. The bridge has been investigated by considering different corrosion scenarios: it has been assumed that the corrosion was spread along one or more elements simultaneously and different percentages of loss area were assumed. More than 1000 scenarios were hence investigated and for each of them, the level of safety of the bridge was assessed by checking: the maximum safety index, SI, of all the elements, the maximum vertical displacement, the elastic buckling multiplier and the modal values and shapes. The main conclusions of the work can be summarized into the following main points:

- when the % of corrosion is low, independently of its position and on the number of simultaneously corroded elements, the

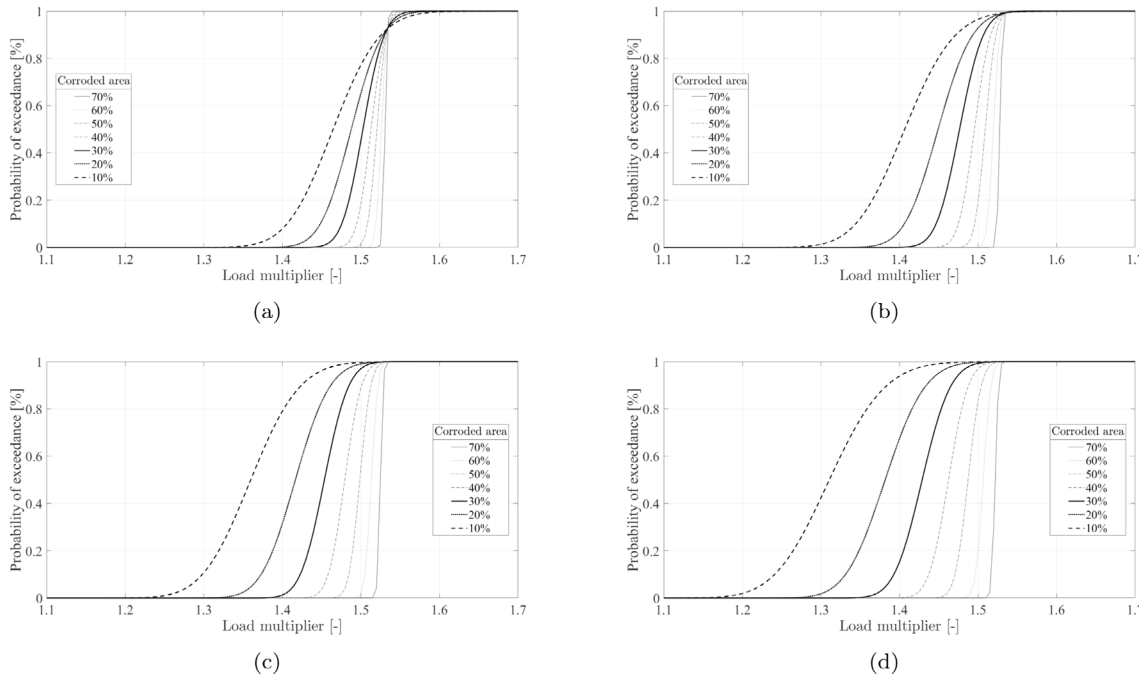

Fig. 18. Mean value of the fragility curves obtained at SLS with one (a), two (b), three (c) and four (d) elements corroded simultaneously.

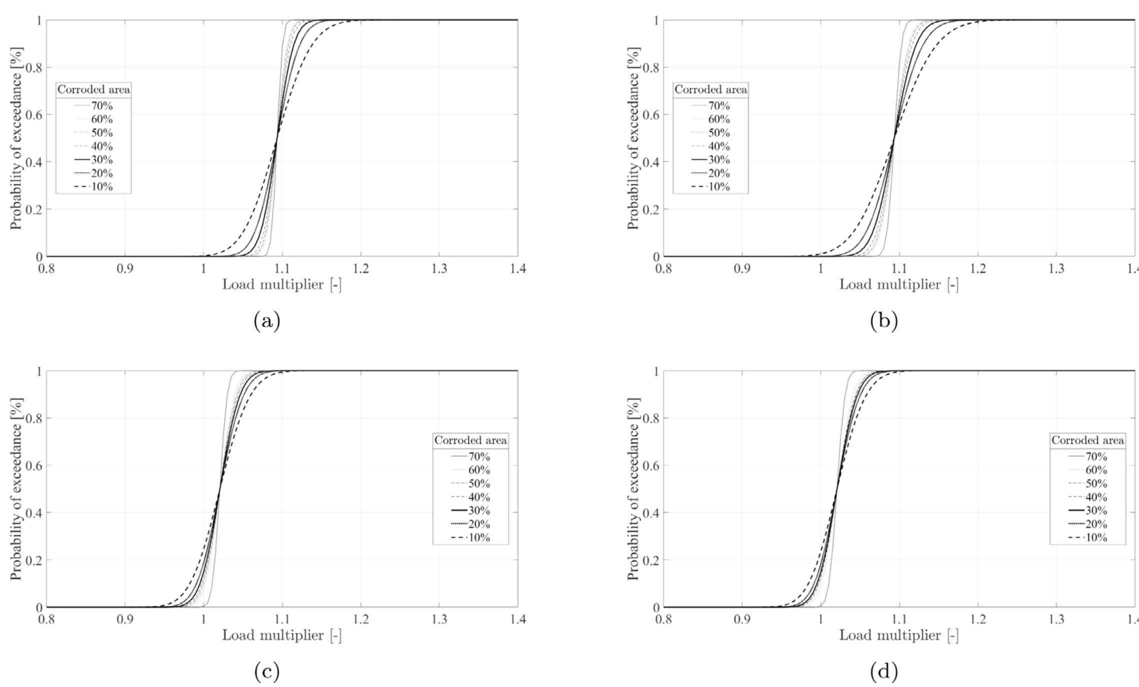

Fig. 19. Mean value of the fragility curves obtained at ULS with one (a), two (b), three (c) and four (d) elements corroded simultaneously.

evaluation of the modal parameters is not able to give a precise prediction on the state of damage of the bridge. On the contrary, global displacements are greatly influenced by corrosion and can give immediate feedback on the bridge's state of damage;

- due to great uncertainties which affect such old structures, it is always suggested to perform a probabilistic assessment of the response. One of the main parameters which should be considered is the material (in terms of Young modulus and yielding stress) which greatly affects the global response.
- The charts can be improved by considering explicitly also the local effects of the corrosion on the elements. Once the charts are created, by means of the probabilistic approach, the conjunction between charts and visual inspections, can give rapid indications to a designer who can carry out a preliminary estimation of the level of safety of the infrastructure.

Finally, the proposed procedure could be extended by considering the local effects of the corrosion: local FE models can be developed by

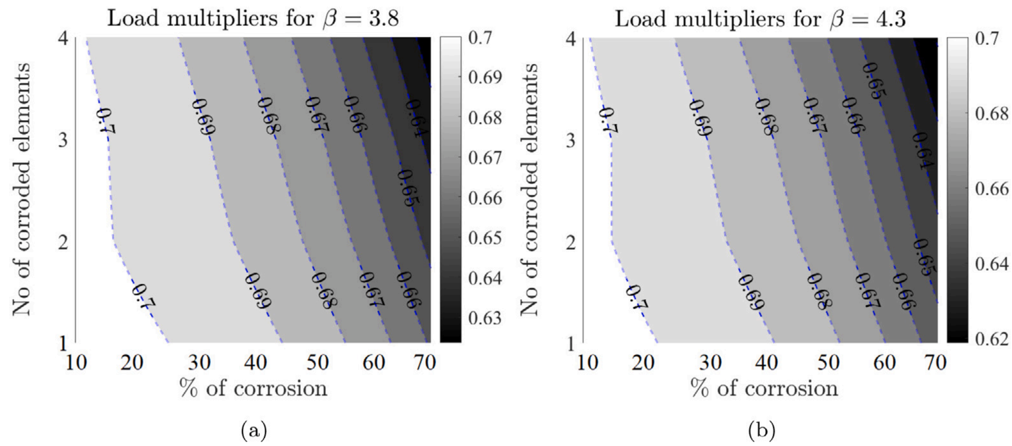

Fig. 20. Contour plot of the load multiplier as a function of the number of corroded elements and the percentage of corrosion corresponding to two values of the reliability indexes 3.8 (a) and 4.2 (b).

implementing the corrosion on the connection, reducing hence the area of nailing.

CRediT authorship contribution statement

Marco Simoncelli: Conceptualization, Methodology, Validation, Formal analysis, Investigation, Data curation, Writing – original draft, Writing and editing, Visualization. **Angelo Aloisio:** Conceptualization, Methodology, Experimental tests, Validation, Formal analysis, Data curation, Writing – original draft, Writing and editing, Visualization. **Marco Zucca:** Data curation, Writing – original draft, Writing and editing, Visualization. **Giorgia Venturi:** Conceptualization, Methodology, Writing – review & editing. **Rocco Alaggio:** Methodology, Resources, Experimental tests, Supervision.

Declaration of competing interest

The authors declare that they have no known competing financial interests or personal relationships that could have appeared to influence the work reported in this paper.

Data availability

Data will be made available on request

References

[1] J.W. Fisher, B.T. Yen, D. Wang, Corrosion and its influence on strength of steel bridge members, Transp. Res. Rec. 1290 (1991) 211–219.
[2] C. Do-Euhn, G.P.R.D, H. Terje, Seismic fragility estimates for reinforced concrete bridges subject to corrosion, Struct. Saf. 31 (2009) 275–283.
[3] A.M. Alani, M. Aboutalebi, G. Kilic, Integrated health assessment strategy using ndt for reinforced concrete bridges, NDT & E Int. 61 (2014) 80–94.
[4] S.A.K. Siti, S.S., J. Adiza, A.A. Muhamad, M.A. Norliyati, Z. Atikah, S. Kunitomo, Vibration-based approach for structural health monitoring of ultra-high-performance concrete bridge, Case Stud. Construct. Mater. 18 (2023) e01752.
[5] G. Venturi, P. Simonsson, P. Collin, Strengthening old steel railway bridges: a review, IABSE Congress Ghent 2021 (2021).
[6] B.T. Svendesen, O. Oiseth, G.T. Froseth, A. Ronnquist, A hybrid structural health monitoring approach for damage detection in steel bridges under simulated environmental conditions using numerical and experimental data, Struct. Health Monit. 22 (1) (2023) 540–561.
[7] M. Venglar, K. Lamperova, M. Sokol, Performance assessment of steel truss railwaybridge with curved track, Acta Polytechnica 62 (5) (2022) 558–566.
[8] A. Kurylowicz-Cudowska, K. Wilde, Fem and experimental investigations of concrete temperature field in the massive stemwall of the bridge abutment, Constr. Build. Mater. 347 (2022) 128565.
[9] X. Han, D. Yang, D.M. Frangopol, Optimum maintenance of deteriorated steel bridges using corrosion resistant steel based on system reliability and life-cycle cost, Eng. Struct. 243 (2021) 112633.
[10] M. Soliman, D. Frangopol, Life-cycle cost evaluation of conventional and corrosion-resistant steel for bridges, J. Bridge Eng. 20 (1–5) (2015) 06014005.
[11] P. Gardoni, K. Mosalam, A. Der Kiureghian, Probabilistic seismic demand models and Fragility estimates for RC bridges, J. Eartquake Eng. 7 (2003) 79–106.
[12] P. Crespi, M. Zucca, M. Valente, On the collapse evaluation of existing RC bridges exposed to corrosion under horizontal loads, Eng. Fail. Anal. 116 (2020) 104727.
[13] P. Crespi, M. Zucca, M. Valente, N. Longarini, Influence of corrosion effects on the seismic capacity of existing RC bridges, Eng. Fail. Anal. 140 (2022) 106546.
[14] N. Adasooriya, S. Siriwardane, Remaining fatigue life estimation of corroded bridge members, Fatigue Fract. Eng. Mater. Struct. 37 (2014) 603–622.
[15] D. Agdas, J.A. Rice, J.R. Martinez, I.R. Lasa, Comparison of visual inspection and structural-health monitoring as bridge condition assessment methods, J. Perform. Construct. Facilities (3) (2016) 04015049.
[16] E. Figueiredo, M.O. Yano, S. da Silva, I. Moldovan, Transfer learning to enhance the damage detectionperformance in bridges when using numerical models, J. Bridge Eng. 28 (1) (2022) e01752.
[17] D.C. Nguyen, M. Salamak, A. Katunin, M. Gerges, Finite element model updating of rc bridge structure with static load testing: A case study of vietnamese thithac bridge in coastal and marine environment, Sensors 22 (2022) 540–561.
[18] J.P. Cheng, P.K.-Y. Wong, H. Luo, M. Wang, P.H. Leung, Vision-based monitoring of site safety compliance based on worker re-identification and personal protective equipment classification, Autom. Constr. 139 (2022) 104312.
[19] M. Moore, B. Phares, B. Graybeal, D. Rolander, G. Washer, Reliability of Visual Inspection for Highway Bridges, Vol. 1, 2001, cited By 1.
[20] J. Ko, Y. Ni, Technology developments in structural health monitoring of large-scale bridges, Eng. Struct. 27 (12) (2005) 1715–1725, SPEC. ISS. cited By 872.
[21] G. Webb, P. Vardanega, C. Middleton, Categories of shm deployments: Technologies and capabilities, J. Bridge Eng. 20 (11) (2015) cited By 98.
[22] S. Yu, D. Li, J. Ou, Digital twin-based structure health hybrid monitoring andfatigue evaluation of orthotropic steel deck in cable-stayedbridge, Struct. Control Health Monit. 29 (8) (2022) e2976.
[23] S. Quqa, P.F. Giordano, M.P. Limongelli, Shared micromobility-driven modal identification of urban bridges, Autom. Constr. 134 (2022) 104048.
[24] R. Sieńko, T. Howiacki, et al., Distributed fibre optic sensing for safety monitoring of concrete, steel and composite bridges, in: Bridge Safety, Maintenance, Management, Life-Cycle, Resilience and Sustainability, CRC Press, 2022, pp. 1612–1620.
[25] D. Liu, W.-M. Gho, J. Yuan, Ultimate capacity of high-strength rectangular concrete-filled steel hollow section stub columns, J. Construct. Steel Res. 59 (12) (2003) 1499–1515.
[26] J. López-Higuera, L. Cobo, A. Incera, A. Cobo, Fiber optic sensors in structural health monitoring, J. Lightwave Technol. 29 (4) (2011) 587–608, cited By 568.
[27] T. Dickens, D. Olawale, G. Sullivan, J. Breaux, O. Okoli, B. Wang, Toward Triboluminescent Sensor Realization for Shm: Statistical Modeling of Triboluminescent Composites, Vol. 7981, 2011, cited By 7.
[28] S. Quqa, Y. Shu, S. Li, K.J. Loh, Pressure mapping using nanocomposite-enhanced foam and machine learning, Front. Mater. 9 (2022) 862796.
[29] A. Aloisio, M.M. Rosso, R. Alaggio, Experimental and analytical investigation into the effect of ballasted track on the dynamic response of railway bridges under moving loads, J. Bridge Eng. 27 (10) (2022) 04022085.
[30] E. Cosser, G. Roberts, X. Meng, A. Dodson, The comparison of single frequency and dual frequency gps for bridge deflection and vibration monitoring, in: Proceedings of the Deformation Measurements and Analysis, 11th International Symposium on Deformation Measurements. International Federation of Surveyors (FIG, 2003, pp. 613–620, cited By 11.

[31] S. Guan, J. Rice, C. Li, G. Wang, Bridge deflection monitoring using small, low-cost radar sensors, 2014, pp. 2853–2862, cited By 9.
[32] T. Chan, D. Ashebo, H. Tam, Y. Yu, T. Chan, P. Lee, E. Perez Gracia, Vertical displacement measurements for bridges using optical fiber sensors and ccd cameras - a preliminary study, Struct. Health Monit. 8 (3) (2009) 243–249, cited By 54.
[33] G. Rossi, R. Marsili, V. Gusella, M. Gioffrè, Comparison between accelerometer and laser vibrometer to measure traffic excited vibrations on bridges, Shock Vib. 9 (1–2) (2002) 11–18, cited By 22.
[34] S. Dorafshan, M. Maguire, N.V. Hoffer, C. Coopmans, Challenges in bridge inspection using small unmanned aerial systems: Results and lessons learned, in: 2017 International Conference on Unmanned Aircraft Systems, ICUAS, IEEE, 2017, pp. 1722–1730.
[35] M.P. Limongelli, C. Gentile, F. Biondini, M. di Prisco, F. Ballio, G. Zonno, P. Borlenghi, S. Bianchi, L. Capacci, M. Anghileri, et al., Bridge structural monitoring: the lombardia regional guidelines, Struct. Infrastruct. Eng. (2022) 1–24.
[36] A. Aloisio, L. Di Battista, R. Alaggio, M. Fragiacomo, Sensitivity analysis of subspace-based damage indicators under changes in ambient excitation covariance, severity and location of damage, Eng. Struct. 208 (2020) 110235.
[37] NTC2018, Norme Tecniche per le Costruzioni, NTC2018, 2018, Ministero delle infrastrutture e dei trasporti, Italy..
[38] A. Aloisio, R. Alaggio, M. Fragiacomo, Time-domain identification of the elastic modulus of simply supported box girders under moving loads: Method and full-scale validation, Eng. Struct. 215 (2020) 110619.
[39] A. Aloisio, R. Alaggio, M. Fragiacomo, Dynamic identification and model updating of full-scale concrete box girders based on the experimental torsional response, Constr. Build. Mater. 264 (2020) 120146.
[40] B. Peeters, G. De Roeck, Reference-based stochastic subspace identification for output-only modal analysis, Mech. Syst. Signal Process. 13 (6) (1999) 855–878.
[41] D.P. Pasca, A. Aloisio, M.M. Rosso, S. Sotiropoulos, Pyoma and pyoma_gui: A python module and software for operational modal analysis, SoftwareX 20 (2022) 101216.
[42] E. Reynders, R. Pintelon, G. De Roeck, Uncertainty bounds on modal parameters obtained from stochastic subspace identification, Mech. Syst. Signal Process. 22 (4) (2008) 948–969.
[43] L. Frỳba, Vibration of Solids and Structures under Moving Loads, Vol. 1, Springer science & business media, 2013.
[44] Eurocode 3, Eurocode 3, EN1993-1-1. Design of Steel Structures—Part 1.1: General Rules and Rules for Buildings, European Committee for Standardization, British Standards Institution, London, UK, 2005.
[45] C. Bernuzzi, M. Simoncelli, Characterization of existing steel racks via dynamic identification, Buildings 11 (603) (2021) 11120603.